ORIGINAL PAPER

Influence of NH−S$^\gamma$ bonding interactions on the structure and dynamics of metallothioneins

Núria Romero-Isart · Baldo Oliva · Milan Vašák

Abstract Mammalian metallothioneins (M$_7^{II}$MTs) show a clustered arrangement of the metal ions and a nonregular protein structure. The solution structures of Cd$_3$-thiolate cluster containing β-domain of mouse β-MT-1 and rat β-MT-2 show high structural similarities, but widely differing structure dynamics. Molecular dynamics simulations revealed a substantially increased number of NH−S$^\gamma$ hydrogen bonds in β-MT-2, features likely responsible for the increased stability of the Cd$_3$-thiolate cluster and the enfolding protein domain. Alterations in the NH−S$^\gamma$ hydrogen-bonding network may provide a rationale for the differences in dynamic properties encountered in the β-domains of MT-1, -2, and -3 isoforms, believed to be essential for their different biological function.

Abbreviations
MT   Metallothionein
β-MT   β-domain of metallothionein

N. Romero-Isart · M. Vašák (✉)
Department of Biochemistry, University of Zürich,
Winterthurerstrasse 190,
CH-8057 Zürich, Switzerland
e-mail: mvasak@bioc.uzh.ch

B. Oliva (✉)
Structural Bioinformatics Lab. (GRIB) Barcelona Research Park of Biomedicine (PRBB), Universitat Pompeu Fabra-IMIM,
08003 Barcelona, Catalonia, Spain
e-mail: boliva@imim.es

MD   Molecular dynamics
RMSD   Root-mean-square deviation
aa   Amino acid
H-bond   Hydrogen bond
NOE   Nuclear Overhauser effect

Introduction

Mammalian metallothioneins (MTs) are metal- and cysteine-rich proteins possessing two sulfur-based metal clusters, formed by the preferential coordination of d^{10} metal ions (Zn(II), Cu(I)) through a conserved array of 20 cysteines. In human, four distinct MT isoforms are known designated MT-1 through MT-4. Whereas MT-1 and MT-2 are found in all tissues, MT-3 is expressed mainly in the brain and MT-4 in cornified and stratified squamous epithelium [1, 2]. MT-3, also known as the growth inhibitory factor (GIF), occurs intra- and extracellularly in the brain and exhibits neuronal growth inhibitory activity in neuronal cell cultures [3]. The present knowledge suggests that MTs can have different functions in a number of biological processes. These include homeostasis and transport of physiologically essential metals (Zn, Cu), detoxification of toxic metals (Cd), protection against oxidative stress, maintenance of intracellular redox balance, regulation of cell proliferation and apoptosis, neuroprotective role, and regulation of neuronal outgrowth [4-7].

The three-dimensional (3D) structure of mouse Cd$_7$MT-1 and Cd$_7$MT-2 from human, rat and rabbit were obtained by NMR spectroscopy [1, 8, 9], but also by X-ray crystallography of rat Cd$_5$Zn$_2$MT-2[10]. The structure reveals a monomeric protein of dumbbell-shape containing two metal-thiolate clusters: a cyclohexane-like 3-metal cluster,

$M^{II}_3 Cys_9$, located in the N-terminal β-domain and an adamantane-like 4-metal cluster, $M^{II}_4 Cys_{11}$, in the C-terminal α-domain. The secondary structure elements in these proteins are limited to numerous half-turns and two short stretches of 3_{10}-helices located in the α-domain. Both the calculated root-mean-square deviation (RMSD) values from NMR data and the crystallographic B-factors indicate that a considerable degree of dynamic structural disorder exists. The experimental data revealed an increased structural mobility of the β-domains when compared to the α-domains in mammalian Cd_7MT-1/-2. Furthermore, despite the average identity between the primary structures of the structurally characterized β-domains of MT-1 and MT-2 of about 80% (Fig. 1) and their high structural similarities (Fig. 2), β-MT-1 shows an increased flexibility compared to β-MT-2. This is best documented for mouse β-MT-1 [9] and rat β-MT-2 [8] with fewer inter-residue NOEs, the absence of slowly exchanging backbone amide protons, and enhanced intersite cadmium exchange rates in the former isoform. Previous molecular dynamics (MD) calculations on $M^{II}_7MT-1/-2$ have explored their conformational behavior showing that the polypeptide loops between cysteine ligands in the β-domain exhibit an extraordinary flexibility without disrupting the geometry of the metal cluster [11-13]. Recently, a considerably enhanced flexibility of the β-domain and the Cd_3-thiolate cluster dynamics of human and mouse Cd_7MT-3 permitted only the solution NMR structure of the α-domain to be determined [14, 15]. Although the generated structural models of β-MT-3 containing the Cd_3-thiolate cluster suggested a similar polypeptide fold to that of β-MT-1/-2 [14, 16], the reason for increased dynamics of β-MT-3 remains unexplained. As the bioactivity of the MT-3 isoform is related to the structure of its β-domain[17, 18], the knowledge of the structural features responsible for the widely differing mobility of the β-domain in MTs is of great interest.

In the present studies, we carried out MD simulations of the available NMR structures of rat β-MT-2 and mouse β-MT-1 with the aim to gain an insight into the structural features responsible for the different domain mobility and the Cd_3-thiolate cluster dynamics in Cd_7MTs.

```
Cd₃β-MT-1  MDP-NCSCSTGGSCTCTSSCACKNCKCTSCK
Cd₃β-MT-2  MDP-NCSCATDGSCSCAGSCKCKQCKCTSCK
Cd₃β-MT-3  MDPETCPCPTGGSCTCSDKCKCKGCKCTNCK
                 *     *    * *    *    *
```

Fig. 1 Aligned amino acid sequences of mouse β−MT-1, rat β−MT-2 and mouse β−MT-3. Differences in the primary structure are highlighted in β−MT-1 and β−MT-2: bold, substitution of residues with similar physico-chemical properties; grey background, polar/non-polar substitution; and white on black background, charged/non-polar substitutions. Terminal metal coordinating cysteines are marked as (*)

Methods

Protein structures

The coordinates of the solution NMR structures of the β-domain of mouse MT-1 (Cd_3-β-MT-1) and rat MT-2 (Cd_3-β-MT-2) were taken from Brookhaven Protein Data Bank (PDB codes: 1DFT [9] and 2MRT [8], respectively). The experimental data were used as initial structures in the molecular dynamics simulations of β-MT-1 and β-MT-2 after energy optimization. Both structures were optimized with the GROMO96 package with 10,000 steps of steepest descent [19].

Parameters used in the molecular dynamics simulations and optimization

Classical MD simulations were performed for each protein embedded by 3500 water molecules in a rectangular box ($41 \times 47 \times 56$ Å^3), using periodic boundary conditions. The standard GROMOS with 43A1 parameters [19-21] was used to calculate the potential energy function along the optimization and molecular dynamics simulation. Charges of sulfur atoms and Lennard Jones parameters of cadmium ions were modified. The charge of cadmium ions and sulfur atoms, and Lennard-Jones parameters (C6 and C12) for cadmium, were taken from the previous publication of Berweger and coworkers [11]. No counter-ions were considered. Other approaches have included cadmium-sulfur bonding experimental data to modify the MM3 force field [13]. However, in our particular case we avoided to use of constraints on cadmium-sulfur bonding in order to be able to explore the underlying basis for differential dynamic properties of the metal-thiolate clusters in MTs. Therefore, we used the classical MD force field from the previous work of Berweger et al. [11]. Of note, there is a novel method for metalloproteins in development by Sakharov and cow. [22, 23] that accounts for the charge transfer and polarization effects.

A twin-range method was used to calculate the non-bonding potential energies. The principal cut-off for the potential energy was set at 8 Å while for long-range interactions we used the reaction field approach and an additional list of interactions within a cut-off of 13 Å around each charged group, updated every 10 steps of simulation, to account for large distance effects [24]. Bond lengths and angles were constrained by SHAKE along the last 9500 steps of the optimization and were kept unconstrained in the initial 500 steps in order to accommodate the structure [25]. Also, position constraints were maintained on the metal cluster (3 cadmium and 9 sulfur atoms) during the first 500 ps of simulation with a harmonical constraint with 4000 kJ mol^{-1} Å^{-2} of force-constant. For the molecular dynamics simulation the time step was 0.002 ps and only stretching

Fig. 2 Left; Superimposition of C^α trace of the N-terminal β-domain of mouse MT-1 (residues 1–30, cyan) and rat MT-2 (residues 1–30, white) as determined by NMR. Superimposition of the Cd_3S_9 clusters in both isoforms is shown in balls and sticks. Right: Metal-thiolate cluster topology with bridging (S_b) and terminal (S_t) sulfur atoms labeled
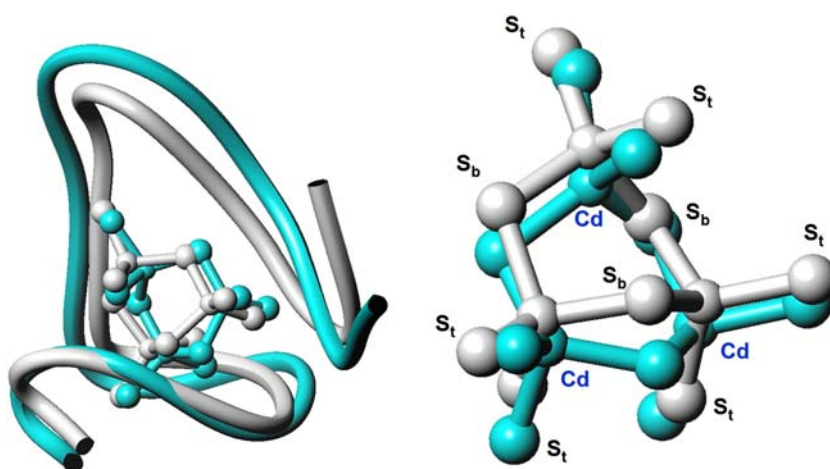
were constrained by SHAKE. Temperature and pressure were maintained respectively at 300 K and 10^5 Pa using a coupling bath.

Analyses of the time-series

The MD simulations were used to explore the conformational space in terms of energy, conformational flexibility and dynamics of the N-terminal β-domains of MT-1 and MT-2 during 5 ns. The structures of the entire N-terminal domain were analyzed by means of atomic-positional root-mean-square deviations (RMSD) curves, calculated for all α-carbon atoms of the domain [26] and by means of the hydrogen bonding pattern. The RMSD values for the backbone and the C^α atoms provide information as to the deformation and the fluctuation of the β-MT structure along the simulation, respectively. Deformation refers to the deviation from the original structure and indicates the degree of malleability. Fluctuation refers to the deviation of the coordinates of C^α atoms with respect to its average position along a time interval of the simulation and indicates the flexibility of a given fragment of the sequence.

The hydrogen bonding pattern was obtained as a time percentage of distances between hydrogen atoms and electronegative atoms (oxygen and sulfur atoms) shorter than 2.8 Å and at the angle between donor and acceptor of proton, centered on the hydrogen atom, between 145° and 215°. Intramolecular NH−S^γ hydrogen bonds involving the hydrogen of peptide nitrogen atoms and coordinating cysteine sulfur atoms have also been analyzed. The reported N-S and H-S distances in small molecules are 3.25–3.55 Å and 2.3–2.8 Å, respectively [27].

The topology and deformation of the Cd_3-thiolate clusters during the simulation has been characterized by the time-averaged distances of the cadmium-sulfur bonds and averaged angles, distinguishing between angles between a metal linked to two bridging sulfurs (*metal ring bridge*, S_b-Cd-S_b), to two terminal sulfurs (*metal terminal angle*,

S_t-Cd-S_t) as well as angle at a metal between terminal and bridging sulfurs (S_t-Cd-S_b). The cluster fluctuation is shown as the standard deviation (SD) around these averages.

The disorder and fluctuation of the Cd_3S_9 metal-thiolate cluster have also been estimated by the virtual entropy calculated using Schlitter's formula and essential dynamics [28-30]. The designation virtual entropy is used to distinguish it from its thermodynamic definition [31]. It was assumed that the Cd_3S_9 cluster is not largely deformed along the simulation, otherwise the calculation would be biased by the matrix used to superpose the conformations from the MD simulation. Therefore, the virtual entropy calculated by Schliter's formula is mainly due to the cluster intrinsic disorder and it is not an artifact of the superimposition with the polypeptide chain. The calculation extracted from the fluctuation matrix of the 12 atoms forming the cluster is translated into energy in kJ mol^{-1} at 300 K. The obtained values give information about the degree of disorder related to the entropy function.

Results

Deviation from the original structure and polypeptide chain fluctuation

Although the average structures of the β-domain in mammalian $Cd_7MT-1/-2$ are very similar [1, 8, 9], substantial differences among their mobility exist. Experimental evidence suggests a markedly increased flexibility of the polypeptide and cluster dynamics in mouse β-MT-1 in comparison with that of rat β-MT-2.

The structural equilibria of β-MT-2 and β-MT-1 polypeptide chains were obtained after the first nanosecond (Fig. 3A). The RMSD values indicate a deformation from the original structure, which can be related to the polypeptide fold flexibility or to the malleability of the conformation. In order to further explore the conformational flexibility of the
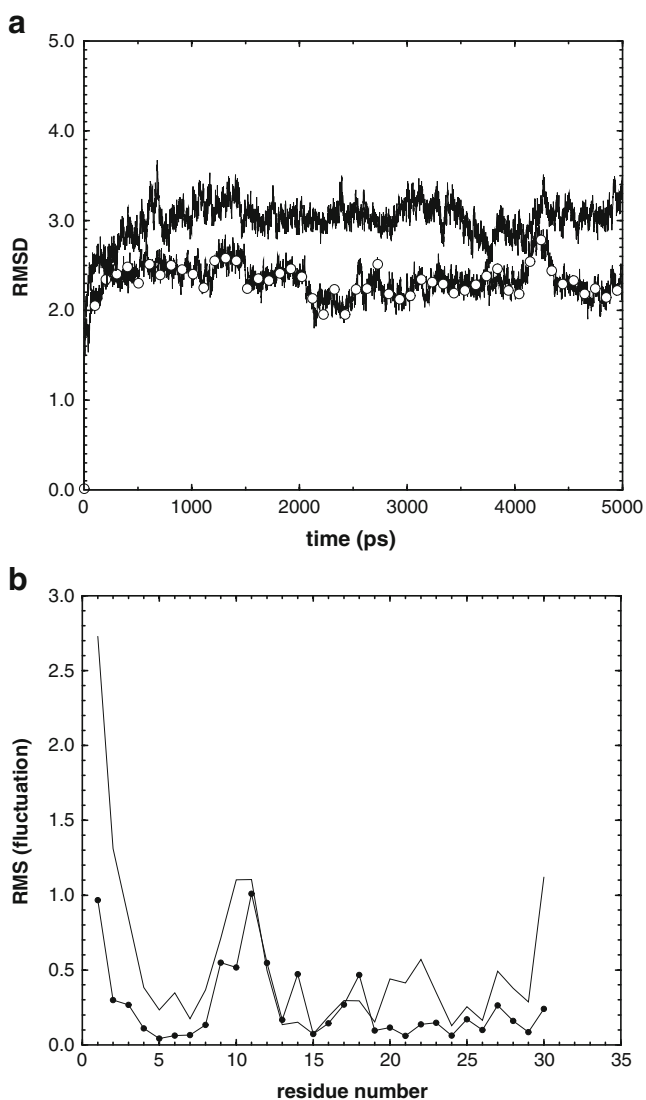
a

b

Fig. 3 (a) Time series (ps) of RMS deviations (Å) of the backbone atoms in Cd$_3$β-MT-1 (continuous line) and Cd$_3$β-MT-2 (line with circles). (b) C$^\alpha$ atom-positional RMS fluctuations (Å) per residue around the averaged structures in the last 4 ns MD simulation of Cd$_3$β-MT-1 (continuous line) and Cd$_3$β-MT-2 (line with full circles)

protein, the positional RMSD for C$^\alpha$ atoms was obtained from atomic fluctuations after the superimposition of structures extracted from the last 4 ns of the trajectory (Fig. 3B). The analysis of the C$^\alpha$ fluctuations shows a larger flexibility of β-MT-1 with respect to β-MT-2, mainly in the N-terminal region of the domain, the fragment near the linker region and in the loop between residues 8 and 12. The experimental structures and the averaged structures after the simulations of β-MT-1 and β-MT-2 are shown in Fig. S1.

Metal-thiolate cluster analysis

The Cd$_3$-thiolate cluster (Cd$_3$S$_9$) in the β-domain of Cd$_7$MT-1/-2 is characterized by a six-membered ring formed by the three cadmium ions and three bridging sulfur atoms with an additional two terminal sulfur atoms involved in the coordination of each cadmium. The deformation of the cluster topology was small in both isoforms and its effect on the six-membered cluster ring was unnoticed, as observed in previous MD simulations [11] (see Table 1). The metal ring bridge angles (S$_b$-M-S$_b$) of the six-membered ring in both isoforms are smaller than the experimental tetrahedral angles due to classical MD parameterization [11].

The virtual entropy values for the Cd$_3$-thiolate cluster of 125 kJ mol^{-1} in β-MT-1 and 96 kJ mol^{-1} in β-MT-2 indicate a larger cluster disorder and internal dynamics in the β-domain of MT-1. In addition, the calculated electrostatic energy between the cadmium ions and the atoms of the polypeptide chain was about 6000 kJ mol^{-1} more stable in β-MT-2 compared to β-MT-1. (Fig. S2). This difference is indicative of a more compact polypeptide enfolding of the Cd$_3$-thiolate cluster in the former isoform.

Hydrogen bonding pattern

The analysis of the set of hydrogen bonds preserved more than 50% of the time along the simulations shows a substantially larger percentage of hydrogen bonds in β-MT-2 than in β-MT-1 (Table 2). The difference between both β-domains arises from the increased number of hydrogen bonds in β-MT-2 between sulfur atoms of terminal metal-coordinated cysteine side-chains and peptide amides (NH−S$^\gamma$). We found six hydrogen bonds of this type in β-MT-2 and only two in β-MT-1. Some prominent hydrogen bonds emerging during the simulations in β-MT-2 with percentages above 75% are Ser6 (NH)—Cys21(S), Cys7(NH)—Cys5(S), Cys15(NH)—Cys13(S), Cys26(NH)—Cys29(S) and Lys30(NH)—Cys29(S). On the other hand, the hydrogen-bonding network in β-MT-1 is more relaxed and less conserved, with only one high-percentage NH−S$^\gamma$ bond occurring between Cys15(NH) and Cys13(S). All NH−S$^\gamma$ hydrogen bonds are to the terminal thiolate ligands possessing a greater electronegativity compared to the bridging thiolates. Moreover, additional hydrogen-bonds involving side-chain atoms are only present in β-MT-2. The H—S distances and NH−S$^\gamma$ angles are similar to those found in other metalloproteins, such as the high-potential iron-sulfur proteins (2.50 Å, 164°) [32] and the Zn$_2$Cys$_6$ cluster of yeast transcription factor GAL4 (2.19–2.63 Å, 149–171°) [33].

The visual comparison presented in Fig. 4 illustrates the NH−S$^\gamma$ hydrogen bonding network in the averaged conformations of βMT-1 and βMT-2 obtained from the last 4 ns of MD simulation.

Table 1 Metal-thiolate cluster topology of Cd_3Cys_9 in β-MT-1 and β-MT-2. Time-averaged and fluctuations (SD) of bond lengths (Å) and bond angles (deg) between bridging (S_b) or terminal (S_t) sulfur atoms Cd_3S_9 — atoms and cadmium ions (Cd). Mean values from the experimental NMR structures have also been calculated for comparison. The calculated virtual entropy shows the local disorder of the cluster

	Entropy (kJ/mol K)	Cd-S_t (Å)	Cd-S_b (Å)	S_t-Cd-S_t (degrees)	S_b-Cd-S_t (degrees)	S_b-Cd-S_b (degrees)
Cd_3β-MT-1	125.0	2.29±0.00	2.61±0.03	117±7	106±3	81±16
Cd_3β-MT-2	96.0	2.23±0.00	2.26±0.00	115±33	106±8	93±6
Cd_3β-MT-1[a]	-	2.50±0.11	2.54±0.01	108±7	108±14	118±6
Cd_3β-MT-2 [b]	-	2.51±0.02	2.57±0.08	110±4	113±2	104±2

[a] Taken from [9]

[b] Taken from [8]

Table 2 Hydrogen-bonding network. Hydrogen bonds present in Cd_3-β-MT-1 and Cd_3-β-MT-2 structures with percentages larger than 50% of hydrogen bond formation between donor and acceptor atoms during the equilibrium time of the simulation (4 ns). NH−S^γ hydrogen bonds are highlighted in bold

Cd_3β-MT-1

Donor Atom		Acceptor Atom		%
5	CYS(N)	23	ASN(O)	86.3
8	SER(N)	25	LYS(O)	53.7
15	**CYS(N)**	**13**	***CYS(S^γ)***	**97.9**
17	SER(N)	14	THR(O)	54.3
18	SER(N)	14	THR(O)	93.8
25	LYS(N)	5	CYS(O)	93.5
28	**SER(N)**	**26**	***CYS(S^γ)***	**54.6**

Cd_3β-MT-2

| Donor Atom		Acceptor Atom		%
4	ASN(N)	2	*ASP(O^δ)*	98.0
5	CYS(N)	2	*ASP(O^δ)*	67.5
6	**SER(N)**	**21**	***CYS(S^γ)***	**99.8**
6	SER(Oγ)	21	CYS(S^γ)	62.7
7	**CYS(N)**	**5**	***CYS(S^γ)***	**98.9**
14	**SER(N)**	**13**	***CYS(S^γ)***	**61.0**
15	**CYS(N)**	**13**	***CYS(S^γ)***	**91.9**
17	GLY(N)	28	SER(O)	68.2
20	LYS(N^ε)[a]	13	CYS(S^γ)	57.0
22	LYS(N)	4	ASN(O)	73.0
23	GLN(N)	4	ASN(O^δ)	61.5
26	**CYS(N)**	**29**	***CYS(S^γ)***	**75.8**
27	THR(N)	30	LYS(Oxt)	57.1
28	SER(N)	26	CYS(O)	81.9
30	**LYS(N)**	**29**	***CYS(S^γ)***	**83.7**
30	LYS(N^ε)[a]	19	CYS(S^γ)	55.0
30	LYS(N^ε)[a]	29	CYS(S^γ)	76.0

[a] For the percentage of H-bonds formed by $N^\varepsilon H_3$ groups, the percentages of the three hydrogen atoms with the same acceptor are summed

Discussion

Experimental evidence shows different structure dynamics of the β-domain of Cd_7MTs which follows the order β-MT-2 < β-MT-1 < β-MT-3. Our MD simulations have reproduced the differences in flexibility of the polypeptide chain and the Cd_3-thiolate cluster between rat β-MT-2 [8] and mouse β-MT-1 [9]. A larger fluctuation of the polypeptide chain in mouse β-MT-1 compared to rat β-MT-2 obtained from the RMSD values are in line with the experimental results. The analyses of topology and the virtual entropy of the Cd_3-thiolate clusters also indicate enhanced cluster dynamics in β-MT-1 than in β-MT-2 (Table 1). The most important finding of our studies are the striking differences in the number of the NH−S^γ hydrogen bonds in β-MT-1 and β-MT-2 (Table 2). While the more flexible β-MT-1 shows only two NH−S^γ hydrogen bonds with more than 50% occurrence, β-MT-2 has six of them, with all but one showing a high occurrence (>75%). Thus, a correlation between the number of NH−S^γ hydrogen bonds and β-domain dynamics exists. Consequently, different dynamic properties exhibited by the β-domain of MT isoforms could be mainly explained by changes in the NH−S^γ hydrogen bonding network. The inspection of differences in amino acid sequences between the β-MT-1 and β-MT-2 isoforms revealed that from the seven substitutions only five confer dissimilar physico-chemical properties (Fig. 1), without altering the overall polarity of the protein (see below). The prominent substitution is that of Asp10 in β-MT-2 by Gly10 in β-MT-1 which produces two contiguous glycine residues as a part of the peptide loop between Cys7 and Cys13 in the latter sequence, conferring a great backbone conformational freedom without any side-chain steric hindrance. Thus, the combination of small sequence differences in the β-domain of MTs may modulate the formation of a NH−S^γ hydrogen-bonding network leading to a greater pliancy and cluster disorder in the β-domain of MT-1.

Fig. 4 NH−S$^\gamma$ hydrogen
bonding network in the aver-
aged conformations of
Cd$_3$βMT-1 (**a**) and Cd$_3$βMT-2
(**b**) obtained from the last 4 ns
of MD simulation. Side-chains
and main-chains of residues in-
volved in NH−S$^\gamma$? hydrogen
bonds are displayed in stick
representation. Metal ions are
shown as white spheres, metal-
thiolate bonds as dotted yellow
lines, and NH−S$^\gamma$? hydrogen
bonds as dotted cyan lines
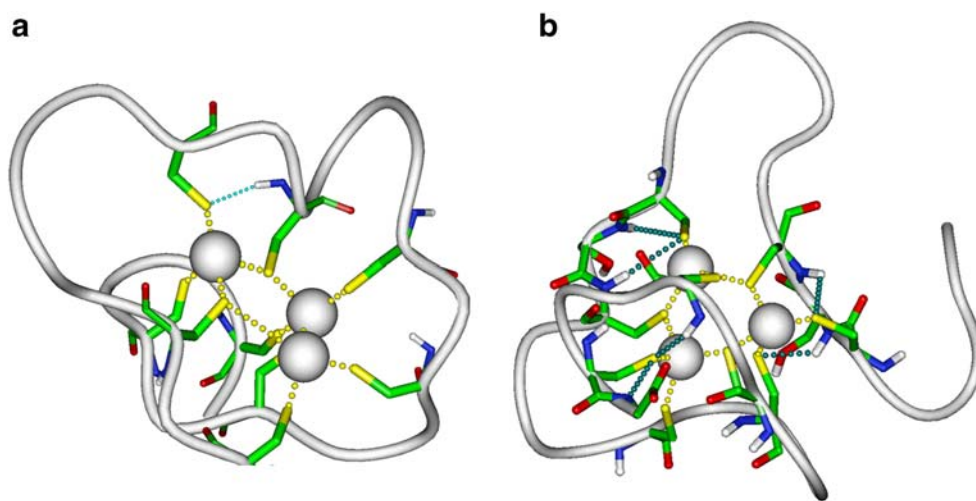
Zangger *et al*. suggested that the higher flexibility and cluster dynamics of β-MT-1 results in part from the reduced electrostatic attractions within this domain and between both domains of MT-1 compared to MT-2 [9]. However, compared to rat β-MT-2, mouse β-MT-1 has one negative (aa 10) and one positive (aa 20) residues less (Fig. 1). Although it would appear that these differences would make β-MT-1 less polar than β-MT-2, further changes between the primary structures of β-MT-1 and β-MT-2, *i.e.*, the substitution of residues Ser8, Thr16, and Ser17 to Ala, Ala, and Gly, respectively, suggests that the differences in polarity should be rather small. In the crystal structure of rat liver Cd$_5$,Zn$_2$MT-2 [10], the greater intersite metal exchange in the β-domain compared to the α-domain observed by NMR, has been discussed in terms of the stabilization of the unligated thiolate state of the cysteine residues by the NH−S$^\gamma$ hydrogen bonds and the distribution of positively charged lysine side chains. However, our MD simulations point to a different structural role of the formed NH−S$^\gamma$ hydrogen-bonding network, *i.e.*, the structural stabilization of the metal-containing β-domain. This can be envisaged as a network of NH−S$^\gamma$ hydrogen bonds buttressing the Cd$_3$-thiolate cluster (Fig. 4). Indeed, the calculated electrostatic energy difference between the polypeptide atoms and Cd(II) ions in β-MT-2 compared to β-MT-1 indicates a tighter polypeptide enfolding of the metal-thiolate cluster in the former, less dynamic isoform, features consistent with the experimental NMR data.

The suggested importance of the NH−S$^\gamma$ hydrogen-bonding network for the dynamics of the β-domain structures in MT-1/-2 is supported by additional simulations performed on the S6P, S8P+T5 mutant of Cd$_3$β-MT-1. Previous biological and structural studies revealed that the engineering of the three critical amino acid residues Thr5, Pro7 and Pro9, present in the conserved T$_5$CPCP$_9$ motif of β-MT-3, into the biologically inactive isoform MT-1 (Fig. 1) brings about not only the neuronal inhibitory

activity, but also a greatly enhanced flexibility of the β-domain and the Cd$_3$-thiolate cluster dynamics not seen in the wild type protein [17]. In our MD simulations four conformations of the β-MT-1 mutant, taking into account all isomeric states of the prolyl residues, were modeled using the structure of Cd$_3$β-MT-1 as the template. It may be noted that the Gly-Gly motif in β-MT-1 is also present in β-MT-3 (Fig. 1). Interestingly, the occurrence of amide NH−S$^\gamma$ hydrogen bonds was dramatically reduced in all these simulations (Table S1). In particular, none of the NH−S$^\gamma$ hydrogen bonds found with more than 50% occurrence in the simulation of β-MT-2 and β-MT-1 (Table 2), occurred in the β-MT-1 mutant with percentages larger than 20%. Furthermore, the loss of NH−S$^\gamma$ hydrogen-bonding interactions in the β-MT-1 mutant was accompanied by the deformation of the Cd$_3$-thiolate cluster and large RMSD deviations and fluctuations of the polypeptide backbone (Table S2 and Fig. S3, Fig. S4)

Within proteins, amide backbone-core NH−S$^\gamma$ hydrogen bonds are often observed to electronically stabilize metal core thiolates, such as in the Zn$_2$Cys$_6$ cluster of yeast transcription factor GAL4 [33], zinc finger proteins [34, 35] and iron-sulfur proteins [36]. In the latter group of proteins, the discovery of NH-S hydrogen bonds to cysteinyl and inorganic sulfur atoms has provided the key information as to our understanding how the biological iron-sulfur clusters differ from their synthetic analogues. This NH−S$^\gamma$ hydrogen bond network also plays an important role in determining the local protein fold and its overall stability as well as the regioselectivity of active-site thiolates in zinc enzymes [37, 38]. Our results reveal another structural attribute of such NH−S$^\gamma$ hydrogen bonds in MTs: the modulation of the Cd$_3$-thiolate cluster dynamics, which has been shown to be critical for the biological activity of MT-3 and, although still enigmatic, may serve a functional role for this class of proteins in the cellular environment.

Conclusions

Our work reproduces the increased structure flexibility of the β-MT-1 when compared to the β-MT-2, as determined by NMR methods. We observe a correlation between the number of backbone amide hydrogen bonds to metal coordinated cysteines and the structure flexibility. Therefore, we propose that NH−S$^{\gamma}$ hydrogen bond interactions are a controlling factor in the regulation of the unique metal-thiolate cluster dynamics of MTs.

References

1. Romero-Isart N, Vašák M (2002) Advances in the structure and chemistry of metallothioneins. J Inorg Biochem 88:388–396
2. Vašák M, Romero-Isart N (2005) In: King RB (ed) Encyclopedia of Inorganic Chemistry, 2nd. Wiley, New York, pp 3208–3221
3. Uchida Y, Takio K, Titani K, Ihara Y, Tomonaga M (1991) The growth inhibitory factor that is deficient in the Alzheimer's disease brain is a 68 amino acid metallothionein-like protein. Neuron 7:337–347
4. Palmiter RD (1998) The elusive function of metallothioneins. Proc Natl Acad Sci USA 95:8428–8430
5. Miles A, Hawksworth G, Beattie J, Rodilla V (2000) Induction, regulation, degradation, and biological significance of mammalian metallothioneins. Crit Rev Biochem Mol Biol 35:35–70
6. Meloni G, Sonois V, Delaine T, Guilloreau L, Gillet A, Teissie J, Faller P, Vašák M (2008) Metal swap between Zn7-metallothionein-3 and amyloid-beta-Cu protects against amyloid-beta toxicity. Nat Chem Biol 4:366–372
7. Hidalgo J, Aschner M, Zatta P, Vašák M (2001) Roles of the metallothionein family of proteins in the central nervous system. Brain Res Bull 55:133–145
8. Schultze P, Wörgötter E, Braun W, Wagner G, Vašák M, Kägi JH, Wüthrich K (1988) Conformation of [Cd7]-metallothionein-2 from rat liver in aqueous solution determined by nuclear magnetic resonance spectroscopy. J Mol Biol 203:251–268
9. Zangger K, Öz G, Otvos JD, Armitage IM (1999) Three-dimensional solution structure of mouse [Cd7]-metallothionein-1 by homonuclear and heteronuclear NMR spectroscopy. Protein Sci 8:2630–2638
10. Robbins AH, McRee DE, Williamson M, Collett SA, Xuong NH, Furey WF, Wang BC, Stout CD (1991) Refined crystal structure of Cd, Zn metallothionein at 2.0 A resolution. J Mol Biol 221:1269–1293
11. Berweger CD, Thiel W, Van Gunsteren WF (2000) Molecular-dynamics simulation of the beta domain of metallothionein with a semi-empirical treatment of the metal core. Proteins 41:299–315
12. Chan J, Huang Z, Merrified M, Salgado M, Stillman M (2002) Studies of metal binding reactions in metallothioneins by spectroscopic, molecular biology, and molecular modeling techniques. Coord Chem Rev 233:319–339
13. Chan J, Merrifield ME, Soldatov AV, Stillman MJ (2005) XAFS spectral analysis of the cadmium coordination geometry in cadmium thiolate clusters in metallothionein. Inorg Chem 44:4923–4933
14. Öz G, Zangger K, Armitage IM (2001) Three-dimensional structure and dynamics of a brain specific growth inhibitory factor:metallothionein-3. Biochem 40:11433–11441
15. Wang H, Zhang Q, Cai B, Li H, Sze KH, Huang ZX, Wu HM, Sun H (2006) Solution structure and dynamics of human metallothionein-3 (MT-3). FEBS Lett 580:795–800
16. Ni FY, Cai B, Ding ZC, Zheng F, Zhang MJ, Wu HM, Sun HZ, Huang ZX (2007) Structural prediction of the beta-domain of metallothionein-3 by molecular dynamics simulation. Proteins 68:255–266
17. Romero-Isart N, Jensen LT, Zerbe O, Winge DR, Vašák M (2002) Engineering of metallothionein-3 neuroinhibitory activity into the inactive isoform metallothionein-1. J Biol Chem 277:37023–37028
18. Hasler DW, Jensen LT, Zerbe O, Winge DR, Vašák M (2000) Effect of the two conserved prolines of human growth inhibitory factor (metallothionein-3) on its biological activity and structure fluctuation: comparison with a mutant protein. Biochem 39:14567–14575
19. Soares TA, Daura X, Oostenbrink C, Smith LJ, Van Gunsteren WF (2004) Validation of the GROMOS force-field parameter set 45Alpha3 against nuclear magnetic resonance data of hen egg lysozyme. J Biomol NMR 30:407–422
20. Daura X, Oliva B, Querol E, Aviles FX, Tapia O (1996) On the sensitivity of MD trajectories to changes in water-protein interaction parameters:the potato carboxypeptidase inhibitor in water as a test case for the GROMOS force field. Proteins 25:89–103
21. Ulrich P, Scott W, Van Gunsteren WF, Torda AE (1997) Protein structure prediction force fields: parametrization with quasi-newtonian dynamics. Proteins 27:367–384
22. Sakharov DV, Lim C (2005) Zn protein simulations including charge transfer and local polarization effects. J Am Chem Soc 127:4921–4929
23. Sakharov DV, Lim C (2009) Force fields including charge transfer and local polarization effects: Application to proteins containing multi/heavy metal ions. J Comput Chem 30:191–202
24. Hünenberger P, Van Gunsteren WF (1998) Alternative schemes for the inclusion of a reaction-field correction into molecular dynamics simulations: Influence on the simulated energetic, structural, and dielectric properties of liquid water. J Chem Phys 108:6117–6134
25. Christen M, Van Gunsteren WF (2005) An approximate but fast method to impose flexible distance constraints in molecular dynamics simulations. J Chem Phys 122:144106
26. Van Gunsteren WF, Karplus M (1981) Effect of constraints, solvent and crystal environment on protein dynamics. Nature 293:677–678
27. Adman E, Watenpaugh KD, Jensen LH (1975) NH—-S hydrogen bonds in Peptococcus aerogenes ferredoxin, Clostridium pasteurianum rubredoxin, and Chromatium high potential iron protein. Proc Natl Acad Sci USA 72:4854–4858
28. Schäfer H, Smith LJ, Mark A, Van Gunsteren WF (2002) Entropy calculations on the molten globule state of a protein: side-chain entropies of a-Lactoalbumin. Proteins 46:215–224
29. Nolde S, Arseniev A, Orekhov VY, Billeter M (2002) Essential domain motions in barnase revealed by MD simulations. Proteins 46:250–258
30. Gargallo R, Hünenberger P, Avilés F, Oliva B, Sci P (2003) Molecular dynamics simulation of highly charged proteins: comparison of the particle-particle particle-mesh and reaction field methods for the calculation of electrostatic interactions. Protein Sci 10:2161–2172
31. Peter C, Oostenbrink C, Van Dorp A, Van Gunsteren WF (2004) Estimating entropies from molecular dynamics simulations. J Chem Phys 120:2652–2661
32. Rayment I, Wesenberg G, Meyer TE, Cusanovich MA, Holden HM (1992) Three-dimensional structure of the high-potential iron-sulfur protein isolated from the purple phototrophic bacterium

Rhodocyclus tenuis determined and refined at 1.5 A resolution. J Mol Biol 228:672–686

33. Marmorstein R, Carey M, Ptashne M, Harrison SC (1992) DNA recognition by GAL4: structure of a protein-DNA complex. Nature 356:408–414

34. Blake PR, Summers MF (1994) Insights into the structural and electronic properties of metalloproteins by heteronuclear magnetic resonance. Adv Inorg Biochem 10:201–228

35. Berg J (1995) Zinc Finger Domains: From Predictions to Design. Acc Chem Res 28:14–19

36. Jensen L (1977) Crystal and Molecular Structure of Rubredoxin from Clostridium pasteurianum. In W Lovenberg (ed) Iron-sulfur proteins Academic Press, New York, p 184

37. Smith JN, Hoffman JT, Shirin Z, Carrano CJ (2005) H-bonding interactions and control of thiolate nucleophilicity and specificity in model complexes of zinc metalloproteins. Inorg Chem 44:2012–2017

38. Maynard AT, Covell DG (2001) Reactivity of zinc finger cores: analysis of protein packing and electrostatic screening. J Am Chem Soc 123:1047–1058